r-Process Calculations and Galactic Chemical Evolution

Shinya Wanajo [a] and Yuhri Ishimaru [b]

[a] *Research Center for the Early Universe, Graduate School of Science, University of Tokyo, Bunkyo-ku, Tokyo 113-8654, Japan; wanajo@resceu.s.u-tokyo.ac.jp*

[b] *Academic Support Center, Kogakuin University, Hachioji, Tokyo 192-0015, Japan; kt13121@ns.kogakuin.ac.jp*

Nuclear Physics A (Special Issue on Nuclear Astrophysics / eds. K. Langanke, F.-K. Thielemann, & M. Wiescher), in press

Abstract

While the origin of r-process nuclei remains a long-standing mystery, recent spectroscopic studies of extremely metal-poor stars in the Galactic halo strongly suggest that it is associated with core-collapse supernovae. In this article, an overview of the recent theoretical studies of the r-process is presented with a special emphasis on the astrophysical scenarios related to core-collapse supernovae. We also review a recent progress of the Galactic chemical evolution studies as well as of the spectroscopic studies of extremely metal-poor halo stars, which provide us important clues to better understanding of the astrophysical r-process site.

Key words: Nuclear reactions, nucleosynthesis, abundances, Stars: abundances, Stars: Population II, Supernovae: general, Galaxy: evolution, Galaxy: halo
PACS: 26.30.+k, 26.50.+x, 97.10.Tk, 97.20.Tr, 97.60.Bw, 98.35.Bd, 98.35.Gi

1 Introduction

The rapid neutron-capture process (r-process) accounts for the production of about half of nuclei heavier than iron, such as the bulk of noble metals (e.g., silver, platinum, and gold) and all actinides (e.g., thorium, uranium, and plutonium). While the basic picture of the r-process, as well as of the slow neutron-capture process (s-process), from the nuclear physics point of view is well established about a half century ago (13; 18), its astrophysical origin has been still unknown. In the last decade, many theoretical efforts have been dedicated to the studies related to the "neutrino wind" scenario,

i.e., the r-process is expected to take place in the high-entropy, neutrino-heated ejecta from the nascent neutron star (NS) in a core-collapse supernova (i.e., Type II/Ibc SNe, 134; 75; 135; 113; 93; 19; 89; 110; 124; 115). A few other scenarios have been also suggested, which include the "prompt explosion" from a low mass SN (111; 126), the "NS merger" (32; 40), and the "collapsar" from a massive progenitor (70; 91). All the scenarios proposed above involve, however, severe problems that remain to be solved, and no consensus has yet been achieved.

Despite difficulties in theoretical studies, recent comprehensive spectroscopic analyses of extremely metal-poor stars in the Galactic halo, aided with Galactic chemical evolution studies, have provided us important clues to the astrophysical origin of r-process nuclei. In particular, discoveries of extremely metal-poor, r-process-enhanced stars with remarkable agreement of their abundance patterns to the scaled solar r-process curve strongly support the idea that the r-process nuclei originate from short-lived massive stars, i.e., core-collapse SNe (108; 20; 44; 109). Furthermore, the observed large star-to-star scatters of r-process elements with respect to iron suggest that the progenitors responsible for the r-process abundance production is limited to a small mass range, when combined with Galactic chemical evolution models (51; 118; 120; 3).

In the subsequent sections, an overview of the current status of explorations of the astrophysical r-process origin is presented from different points of views, i.e., nucleosynthesis studies related to, in particular, core-collapse SNe (§ 1), and chemical evolution studies of the Galactic halo, along with recent spectroscopic analyses of extremely metal-poor stars (§ 2). Conclusions follow (§ 3).

2 r-Process Calculations

The r-process proceeds through the neutron-rich region far from β-stability in the nuclide chart (Fig. 1), which needs a high neutron-to-seed abundance ratio (≥ 100, where "seed" is the heavy nuclei with $A \sim 60 - 90$) at the beginning of the r-process phase ($T_9 \sim 3$, where $T_9 \equiv T/10^9$ K and T is temperature). The requirements on the physical conditions here are threefold – low electron fraction (Y_e, number of protons per baryon), high entropy ($S \propto T^3/\rho$ in radiation dominated matter, where ρ is mass density), and short dynamic timescale (e.g., $\tau_{\rm dyn} = |\rho/(d\rho/dt)|_{T=0.5{\rm MeV}}$). Matter with $Y_e < 0.5$ is called *neutron rich*. In particular, the matter with $Y_e < 0.3$ contains free neutrons even in the nuclear statistical equilibrium (NSE) at relatively low temperature. Hence, the matter with significantly low Y_e, say, < 0.2, may naturally lead to robust r-processing, less dependent on S and $\tau_{\rm dyn}$. Even if the matter is only moderately neutron-rich, say, $Y_e \sim 0.4$, sufficiently high S

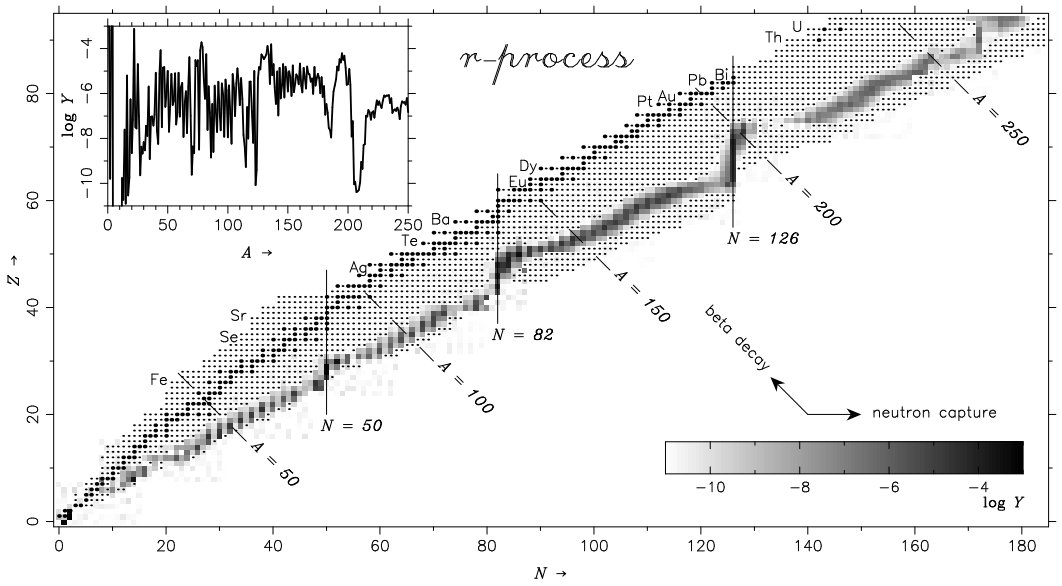

Fig. 1. Snapshot of the nucleosynthesis calculation at the end of the r-process phase. The abundances are shown by the grey image in the nuclide chart. The abundance curve as a function of mass number is shown in the upper left. The nuclei included in the reaction network are denoted by dots, with the stable and long-lived isotopes represented by large dots (125).

($>$ a few $100N_Ak$) or short $\tau_{\rm dyn}$ ($<$ a few 10 ms) inhibit free nucleons and α-particles to assemble to heavier nuclei during the α-process phase ($T_9 \approx 7-3$), and may leave sufficient free neutrons needed for a successful r-process. Our main goal is to find such physical conditions by (to some extent) realistic astrophysical modelings.

2.1 Neutrino Wind

The bottleneck reaction from light ($Z < 6$) to heavy ($Z \geq 6$) nuclei in the neutron-rich environment is the three-body interaction, $\alpha(\alpha n, \gamma)^9$Be followed by ^{9}Be$(\alpha, n)^{12}$C, whose rate is proportional to ρ^2. This is why higher S (i.e., lower ρ in the radiative condition) is favored for r-process, which tends to leave more free neutrons. Such high entropy is expected to realize in the neutrino-heated ejecta ("neutrino wind") from the nascent NS in a core-collapse SN, and many efforts have been devoted to the study of this scenario in the last decade. Woosley et al. (135) have demonstrated that an excellent fit to the solar r-process abundance curve is obtained in their nucleosynthesis calculations with the thermodynamic trajectories from the hydrodynamic simulation of a $20M_\odot$ "delayed" SN explosion. The high entropy ($\sim 400N_Ak$) that led to a successful r-processing was not, however, duplicated by subsequent theoretical studies (113; 93). In the following, the current status of the theoretical studies of the neutrino wind is described based on our recent works (89; 124; 125) that result

in similar conclusions to other studies (93; 19; 110; 115).

2.1.1 Wind Properties and Nucleosynthesis

After several 100 ms from the core bounce, the hot convective bubbles are evacuated from the proto-NS surface, and the winds driven by neutrino heating emerge, as can be seen in some hydrodynamic simulations of "successful" delayed SN explosions (e.g., 135; 12). During this wind phase, a steady flow approximation may be justified. Assuming the spherical symmetry, the equations of baryon, momentum, and mass-energy conservation with the Schwarzschild metric (e.g., equations (1)-(3) in 124) can be solved numerically. Thus, once the NS mass (M), the neutrino sphere radius (R_ν), and the neutrino luminosity (L_ν) are specified along with the mass ejection rate ($\dot{M}$) as the boundary condition, the wind solution can be obtained.

Figs. 2a-c show the maximum mass ejection rate ($\dot{M}_{\rm max}$, i.e., for transonic solutions), the entropy per baryon (S/k at $T = 0.5$ MeV), and the timescale (τ, as the time for material to cool from $T = 0.5$ to 0.2 MeV as a measure of the duration of the seed abundance production), respectively, as functions of L_ν that is assumed to be equal for all neutrino flavors (124). The results are compared to those with post-Newtonian corrections (93) and with fully general relativistic hydrodynamic calculations (110), which are in good agreement each other. As can be seen, the entropy is $\sim 120 N_A k$ at $L_\nu = 10^{51}$ erg s^{-1} for $M = 1.4 M_\odot$ and $R_\nu = 10$ km (model A, dot-dashed line), which is more than three times smaller than that in Woosley et al. (135). However, the entropy can be $\sim 200 N_A k$ for a very *compact* proto-NS, i.e., $M = 1.4 M_\odot$ and $R_\nu = 7$ km (model B, dashed line) or, $M = 2.0 M_\odot$ and $R_\nu = 10$ km (model C, solid line), where the general relativistic effects are of particular importance. Not only to the entropy, the general relativity helps to reduce τ as can be seen in Fig. 2c.

The yields of r-process nuclei are obtained by application of an extensive nuclear reaction network that consists of ~ 5000 species along with all relevant nuclear reaction and weak rates (Fig. 1, see 124; 125; 126; 127, for the nuclear data inputs). The results for the above three models are shown in Fig. 3, where Y_e is taken to be 0.4 and the abundances for constant L_ν's are mass-averaged assuming a time evolution of L_ν from 4×10^{52} to 1×10^{51} erg s^{-1} (see 124; 125, for more detail). For a *typical* proto-NS (model A), only the nuclei between the first ($A = 80$) and second ($A = 130$) r-process peaks are produced, owing to its insufficient entropy. In contrast, for very *compact* proto-NSs (models B and C), the third r-process peak ($A = 195$) forms and each abundance curve is in reasonable agreement with the solar r-process abundance distribution. This is not only due to the moderately high entropy ($\sim 100 - 200 N_A k$), which is still a half that in Woosley et al. (135), but to the short timescale ($\tau \leq 10$ ms) when L_ν is still high and thus $\dot{M}$ is large, as can be seen in Fig. 2. The third

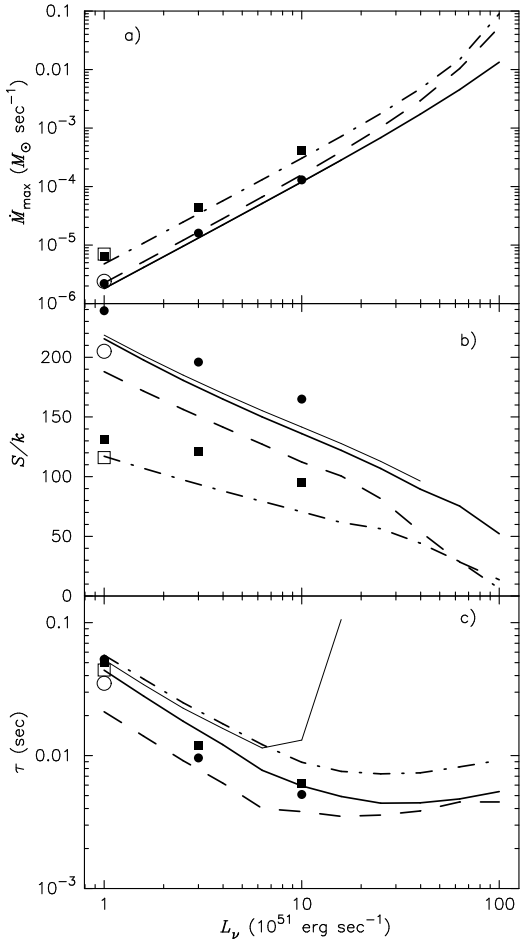

Fig. 2. (a) The maximum mass ejection rates, (b) entropies, and (c) timescales for models A (dot-dashed line), B (dashed line), and C (thick-solid line), as functions of L_ν for the transonic winds. The thin-solid lines are for the subsonic wind with $\dot{M} = 0.995 \times \dot{M}_{\rm max}$ for model C. Also denoted are the results from (110) (filled squares and circles) and (93) (open squares and circles). The squares and circles are the results with the same model parameters M and R_ν as the models A and B, respectively.

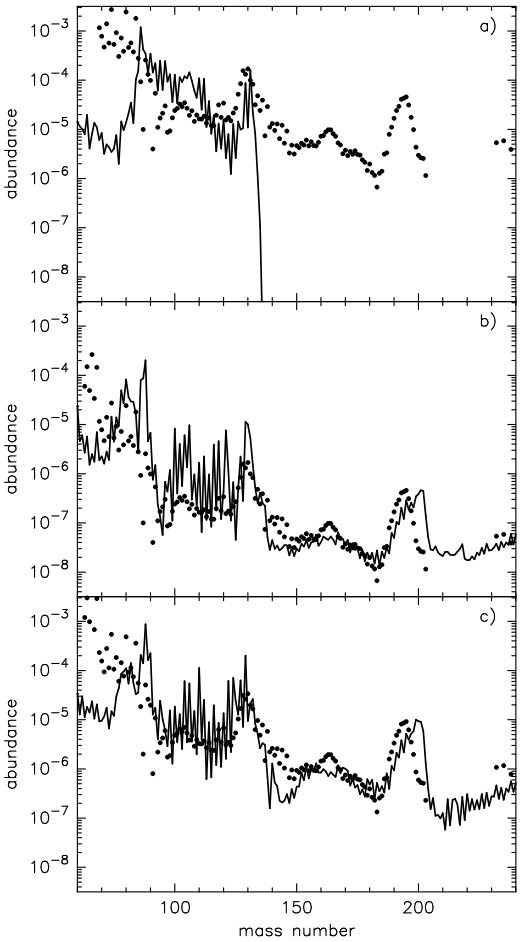

Fig. 3. The mass-weighted integrated yields for models A (a), B (b), and C (c) as functions of mass number (lines). Also denoted are the scaled solar r-process abundances (61) (points), which are scaled to match the heights of the second (a) and third (b and c) r-process peaks, respectively. For model A, only the nuclei between the first and second r-process peaks are produced. The third peak is formed for models B and C. Note a significant overproduction of nuclei near $A = 90$ for both (b) and (c).

peak formation can be seen only for the proto-NS with $M \geq 1.9 M_\odot$ (with $R_\nu = 10$ km, 124), which (if exist) might further collapse to a black hole. The ejecta mass of r-processed material per event for model C is estimated to be $\sim 1 \times 10^{-4} M_\odot$, which is in good agreement with the requisit amount obtained from Galactic chemical evolution studies (51; 53).

It should be noted that R_ν might be significantly larger than 10 km as-

sumed here (for models A and C), in particular at an early phase with $L_\nu >$ several 10^{51} erg s^{-1} (depending on the equation of state for the nuclear matter (EOS) applied, 135; 92), which would result in lower S and longer τ. Hence the results shown in Fig. 3 do not guarantee the third peak formation for $M = 2.0 M_\odot$ (nor the second peak formation for $M = 1.4 M_\odot$). This should be taken as the *minimum* requisite mass (or compactness M/R_ν) of the proto-NS in order to obtain the third r-process peak abundances.

2.1.2 Neutrino Effects on Nucleosynthesis

Possible effects of neutrino interactions on the r-process have been extensively investigated by a number of authors (76; 78; 79; 80; 81; 94; 77; 124; 64; 114). When restricted to the physical conditions deduced from the "realistic" modelings of neutrino winds, however, the major contributors to the r-process would be only the neutrino interactions on free nucleons and on α particles. Other effects, i.e., the neutrino interactions on heavy nuclei and subsequent neutron emission (or fission), are estimated to be small because of their small cross sections (e.g., 114), which might be buried with large uncertainties in, e.g., nuclear physics far from β-stability as well as astrophysical conditions (e.g., 127).

The neutrino capture on free nucleons affects the r-process by changing Y_e – so called the "α effect" (78; 80; 77). As the temperature decreases to $T_9 \sim 7$, α particles form by assembling from free neutrons and protons, while the number ratio of free neutrons to free protons is locked by neutrino capture on free nucleons in the intense neutrino flux. As a result, the formation of α particles continues and Y_e approaches ~ 0.5, which may hinder the r-process (77). This plays, however, only a minor (but non-negligible) role in the "realistic" neutrino winds. For example, the increase of Y_e ($= 0.40$, initially) from $T_9 =$ 9 to 2.5 (at the onset of r-process) is no more than 0.03 for the winds in model C (§ 2.1.1). Note that this effect is of importance only at later phase ($L_\nu <$ several 10^{51} erg s^{-1}), where the longer dynamic timescale as well as the shorter distance from the neutrino sphere at $T_9 \sim 7$ results in relatively larger neutrino fluence regardless of the lower L_ν (see Fig. 2c).

Neutrino spallation reactions on ^{4}He may also affect the nucleosynthesis because of the large abundance of α particles in the high-entropy wind (76). This is due to the increase of seed abundances even after the freezeout of three-body (i.e., $\alpha(\alpha n, \gamma)^9$Be and $\alpha(\alpha\alpha, \gamma)^{12}$C) reactions at $T_9 \sim 3$, through the two-body reaction pathways opened up by the spallations, e.g., $\alpha(\nu, \nu' p)^3$H followed by ^{3}H$(\alpha, \gamma)^7$Li and further α capture. As a result, the r-process may be significantly hindered owing to the reduced neutron-to-seed ratio, although its efficiency is highly dependent on the neutrino spectra and luminosities as well as on the fluid dynamics near the proto-neutron star (76; 114). Note

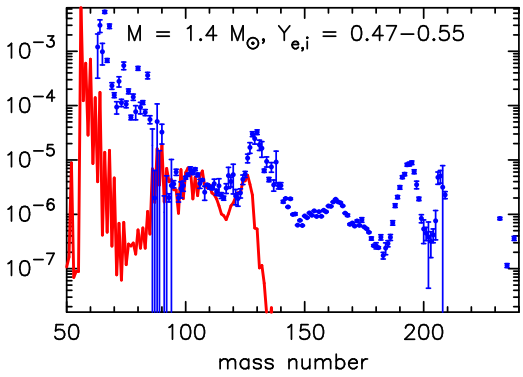

Fig. 4. The final abundances as a function of mass number averaged by the ejected mass and Y_e (see text) for $M = 1.4M_\odot$. Also denoted are the scaled solar r-process abundances (points).

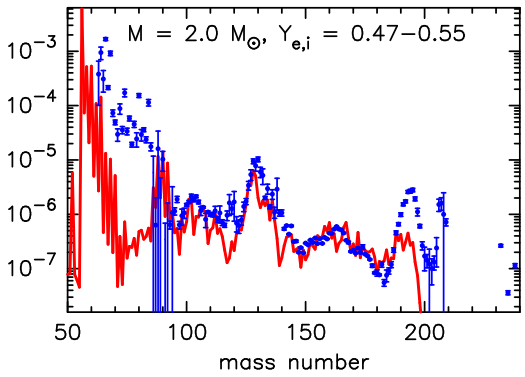

Fig. 5. Same as Fig. 4, but for $M = 2.0M_\odot$.

that neutrino spallations of neutrons, $\alpha(\nu, \nu' n)^3$He, have no effect on the nucleosyntheis in neutron-rich environment, which is immediately followed by ^{3}He$(n, \gamma)\alpha$ (76).

2.1.3 Overproduction Problem

As can be seen in Figs. 3b-c and in many other "successful" r-process calculations, one worrisome aspect of the neutrino wind scenario is a large overproduction of $N = 50$ (closed neutron shell, $A \approx 90$) nuclei synthesized through α-process by a factor of $10-100$ (e.g., 135; 124). This originates from the moderately high entropy ($50-100N_Ak$) ejecta with a large $\dot{M}$ before the r-process epoch ($L_\nu > 10^{52}$ erg s^{-1}) (Fig. 2). The overproduction diminishes when decreasing the neutron richness in the wind to $Y_e \sim 0.49$ (47; 31; 125). This is due to the termination of α-process by photodisintegration at $N \approx Z \approx 28$ rather than $N \approx 50$. Instead, some interesting isotopes ^{64}Zn, ^{70}Ge, and light p-process nuclei ^{74}Se, ^{78}Kr, ^{84}Sr, and ^{92}Mo are produced (47; 128), which seem difficult to be fulfilled by other astrophysical sites (but see possible explanations for ^{64}Zn, 121; 92). In fact, recent detailed hydrodynamic simulations of "successful" SN explosions with accurate neutrino transport show that Y_e at early times is close to 0.5 or even higher (92; 33; 12). For example, a two-dimensional hydrodynamic simulation by Buras et al. (12) shows that the Y_e values in the neutrino-processed ejecta during the early phase of the explosion distribute between 0.47 and 0.56 with the maximum amount at ~ 0.50.

As an excises, the nucleosynthesis results with the variation of Y_e are presented, which was assumed to be a constant value ($= 0.40$) in § 2.1 (for a more detailed discussion, see 128). Here, the initial Y_e is assumed to be constant (Y_{e0}) for $t_0 < t \leq t_1$ and $Y_e(t) = (Y_{e0} - Y_{ef})(t/t_1)^{-1} + Y_{ef}$ for $t > t_1$, where $t_1 = 2$ s and $Y_{ef} = 0.35$, which mimics the hydrodynamic results in Woosley et al. (135).

The values of Y_{e0} are taken to be from 0.47 to 0.55 (nine cases) according to Buras et al. (12), instead of ~ 0.46 in Woosley et al. (135). The mass-averaged nucleosynthesis results as in § 2.1 are further Y_e-averaged with the Y_{e0} distribution of neutrino-processed ejecta obtained by Buras et al. (12, Fig. 38). The final abundance curve is shown in Figs. 4 and 5 as a function of mass number, which is compared to the scaled solar r-process abundances.

As can be seen, no overproduction of the $A \approx 90$ nuclei appears in this abundance curve for both $M = 1.4M_\odot$ and $2.0M_\odot$ cases. In fact, the harmful overproduction at $N = 50$ is now replaced with the appropriate production of the p-nuclei ^{92}Mo (128). This is due to the dominance of the matter with $Y_{e0} \geq 0.49$ at the early phase of neutrino winds assumed here. However, the amount of the r-processed material seen in Fig. 5 is about one order smaller (and the third peak abundances are also deficient in this case) than that in Figure 3c, since the r-process does not take place when L_ν is high (and thus $\dot{M}$ is large) as in § 2.1, owing to the high Y_e at the early phase. Given the neutrino wind is the major production site of the r-process nuclei, therefore, it is not evident if merely the proton richness in the neutrino-heated ejecta at the early phase solves the overproduction problem.

2.1.4 Is the Answer "Blowing in the Wind"?

A most probable implication is that the neutrino winds from a *typical* proto-NS (e.g., $M = 1.4M_\odot$ and $R_\nu = 10$ km) are responsible for the production of *only* light r-process nuclei such as Sr, Y, and Zr, and no heavier than the second peak ($A = 130$) as can be seen in Fig. 3a, with some interesting isotopes (e.g., ^{64}Zn, ^{70}Ge, and light p-process nuclei) between $A = 60$ and 100 (128). This is still of importance, however, since there are increasing evidences that at least two different astrophysical sites exist for the origins of "light" and "heavy" r-process nuclei (see § 3.3). Nevertheless, a possibility of the production of species beyond the second ($A = 130$) and third ($A = 195$) peaks with a very *compact* proto-NS (e.g, $M/R_\nu = 0.2M_\odot$/km as for models B and C in Figs. 2 and 3) cannot be ruled out. In fact, many EOSs meet this condition, $M/R_\nu \approx 0.2M_\odot$/km, near their maximum masses ($M \approx 2.0 - 2.3M_\odot$, see 66; 124). Recent measurements of NS masses in binary systems also support the presence of such massive NSs (67). It should be noted that a proto-NS's mass could be slightly larger than the maximum mass of a cold star because of its extra leptons and thermal energy. In this case, collapse to a black hole would take place (after the r-process) on a diffusion time of a few 10 s, which might have occured in SN 1987A (67).

If the neutrino winds were *really* the major production site of the heavy r-process nuclei, therefore, the progenitor would have a relatively large mass, e.g., $\geq 20M_\odot$. On the other hand, the lighter r-process nuclei would be sup-

plied from low mass progenitors ($\sim 10 - 15 M_\odot$). This difference may reflect the change of a core structure with the progenitor mass, i.e., the steep density gradient with the small iron core ($\sim 1.3 M_\odot$) for a star of $\leq 15 M_\odot$ and the mild density gradient with the massive iron core ($\sim 1.8 M_\odot$) for a star of $\geq 20 M_\odot$ (17). It should be noted that the very massive progenitors would suffer from a significant "fallback" of the matter once ejected, resulting in, perhaps, no ejection of r-processed material (115). Hence, the progenitors for the origin of the heavy r-process nuclei may be limited to a small mass range, e.g., $20 - 25 M_\odot$. This would make such an event relatively rare, accounting only about 10% of all core-collapse SN events. This (moderate) rareness does not cause a problem, but rather is needed from Galactic chemical evolution as discussed in § 3.2.

It should be emphasized that the implications above are all based on the assumption of spherical symmetry as well as on the arbitrary chosen Y_e. There have been no qualitative studies of r-process in asymmetric neutrino winds nor with an accurate determination of Y_e. Therefore, conclusions described here might be modified by the future works based on more *realistic* modelings of neutrino winds with multidimensional hydrodynamics as well as with an accurate treatment of neutrino transport. It is interesting to note that recent two-dimensional simulations demonstrate that hydrodynamic instabilities can lead to low-mode ($l = 1, 2$) asymmetries of the fluid flow in the neutrino-heated layer behind the SN shock (104; 57). This provides not only a natural explanation for aspherical mass ejection and for pulsar kicks but shows some promise as the yet unknown explosion mechanism of core-collapse SNe (57). Such multi-dimensional effects may have to be taken into account in the future work, since the r-process takes place relatively close to the core ($\sim 100 -$ 1000 km) where the asymmetry plays a significant role. The strong magnetic field ("magneter-like" strength such as $\sim 10^{15}$ G, three orders of magnitude larger than the typical value) in a proto-NS has been also suggested to increase entropy and thus help the r-process even with $M \approx 1.4 M_\odot$ (116; 112) (but see 55). Such SN events account for no more than a few % of all SN events. This might be, however, still in reasonable agreement with the constraint from Galactic chemical evolution (§ 3.2).

2.2 Prompt Explosion

If a massive star explodes hydrodynamically at core bounce prior to the delayed neutrino heating, the ejecta keeps its neutron richness due to electron capture, $Y_e \sim 0.2$, which may lead naturally to r-processing regardless of the relatively low entropy, $S \sim 10 N_A k$ (105; 102; 45). This is one of the reasons that this scenario, "prompt explosion" has been still considered to be a possible explanation for the r-process origin (132; 111; 126), despite difficulties in

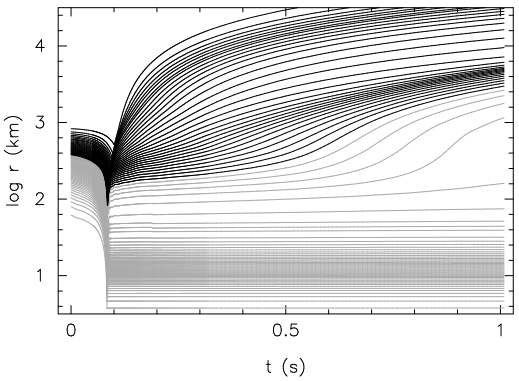

Fig. 6. Time variations of radius for selected mass points in the prompt explosion of a $9M_\odot$ star, in which the shock-heating energy is enhanced *artificially* by a factor of 1.6.

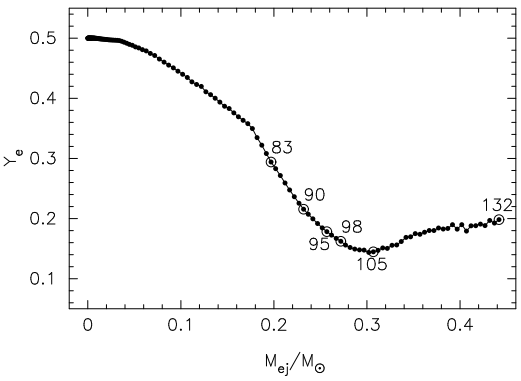

Fig. 7. Y_e distribution in the ejected material. The surface of the O-Ne-Mg core is at mass coordinate zero. Some selected mass points are denoted by zone numbers (see Fig. 8).

achieving such an explosion by self-consistent hydrodynamic calculations. In fact, many previous works have suggested that even the SNe near their lower-mass end ($\sim 10M_\odot$), which form small iron cores ($\sim 1.3M_\odot$), have difficulties in achieving hydrodynamic explosions (9; 15; 16; 10; 11; 8). Optimistically saying, a prompt explosion may occur in the collapse of the *lowest* mass progenitor, perhaps an $8-10M_\odot$ star that forms an O-Ne-Mg core at its center, owing to its small gravitational potential as well as the small NSE core at the onset of core bounce (84; 46; 82).

It should be noted that recent detailed core-collapse simulations of the $9M_\odot$ star having an O-Ne-Mg core with accurate treatment of neutrino transport (68; 57) do not confirm the prompt explosion found in a previous study with simpler neutrino treatment (46). Instead, a weak explosion by delayed neutrino-heating emerges (this is only one case that a one-dimensional self-consistent simulation with accurate neutrino transport results in an explosion, 57). In addition, the fate of the stars in this mass range is quite uncertain, which is highly dependent on the treatment of the convection as well as the mass loss assumed in the calculations of stellar evolution. In particular, an efficient mass loss would result in losing whole the envelope before reaching the Chandrasekhar mass and then leaving an O-Ne-Mg white dwarf (84). As a result, the mass range of the stars that undergo SNe would be restricted between $M_{\rm WD}$ and $10M_\odot$, where $8M_\odot \leq M_{\rm WD} \leq 10M_\odot$ (see also recent studies 97; 50; 98; 28). A limited mass range, say, between $M_{\rm WD} = 9.5M_\odot$ and $10M_\odot$, still accounts for about $7-8\%$ of all core-collapse SN events, which is in good agreement with a constraint from Galactic chemical evolution (§ 3.2). Hence, comprehensive studies including stellar evolutions covering whole this mass range, as well as the subsequent core-collapse simulations, are awaited before drawing any final conclusions. In the meantime, however, it would be valuable to examine the r-process nucleosynthesis in a *schematic* prompt ex-

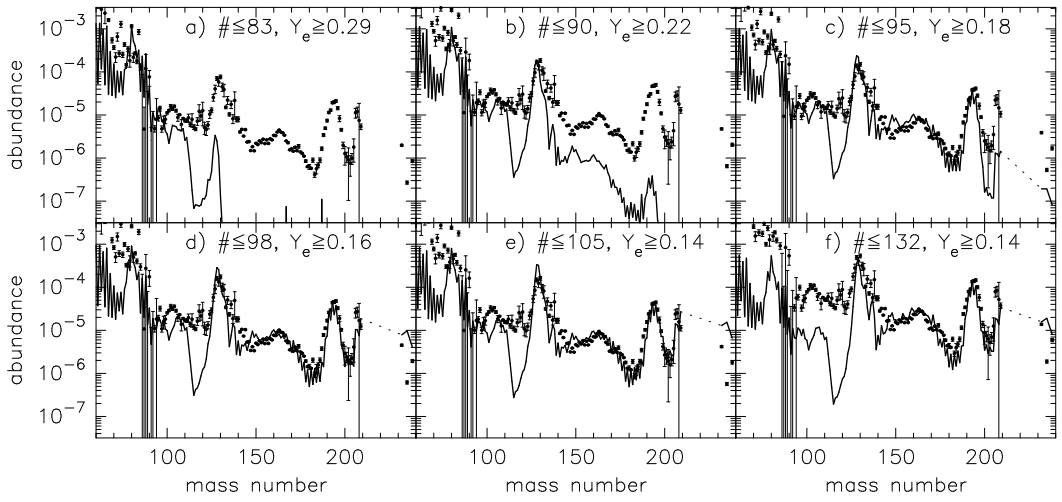

Fig. 8. Mass-averaged r-process abundances (line) as a function of mass number obtained from the ejected zones in (a) ≤ 83, (b) ≤ 90, (c) ≤ 95, (d) ≤ 98, (e) ≤ 105, and (f) ≤ 132 (see Fig. 7). These are compared with the solar r-process abundances (points) (61), which is scaled to match the height of the first peak ($A = 80$) for (a), the second peak ($A = 130$) for (b), and the third peak ($A = 195$) for (c)-(f).

plosion forced by, e.g., enhancing shock-heating energy (126) or suppressing electron capture (111). In the following, our recent result on the r-process in a collapsing O-Ne-Mg core (126) is briefly presented (see also 111).

A *purely* hydrodynamical (i.e., without neutrino) core-collapse simulation of a $9M_\odot$ star (84) that forms a 1.38 $M_\odot$ O-Ne-Mg core is performed with a one-dimensional implicit Lagrangian hydrodynamic code with Newtonian gravity. Major input physics is the equations of state of nuclear matter (EOS) (106) and of the electron (and positron) gas with arbitrary relativistic pairs as well as arbitrary degeneracy, and electron (and positron) capture on free nucleons and nuclei (65). The capture is suppressed above $\rho = 3 \times 10^{11}$g cm^{-3} to mimic the *neutrino trapping*. The composition of the O-Ne-Mg core is held fixed until the temperature reaches $T_9 = 2$ that is taken to be the onset of oxygen burning, at which point the matter is assumed to instantaneously be in NSE. We find that only a weak explosion results with the explosion energy of $E_{\rm exp} = 1.8 \times 10^{49}$ ergs, where the minimum Y_e is only 0.45 and no r-processing is expected. In order to examine the possible operation of the r-process in this star, an energetic explosion ($E_{\rm exp} = 3.5 \times 10^{51}$ ergs) is *artificially* obtained by multiplying a factor of 1.6 to the shock-heating term in the energy equation (Fig. 6). The highly neutron-rich matter ($Y_e \approx 0.14$, Fig. 7) from deeper inside of the core is ejected, which results in robust r-processing as can be seen below.

The yields of r-process nuclei obtained with the nuclear reaction network (Fig. 1) are mass-averaged from the surface (zone 1) to the zones (a) 83, (b) 90, (c) 95, (d) 98, (e) 105, and (f) 132 (see Fig. 7), which are compared with the solar r-process abundances (61) as can be seen in Fig. 8. A solar r-process

pattern for $A \geq 130$ is naturally reproduced in cases c-f, owing to the ejection of highly neutron-rich matter ($Y_e < 0.20$). On the other hand, the solar-like abundance curves up to $A \approx 100$ and 130 in cases a and b, respectively, can be seen. Note that a problematic overproduction of $N = 50$ ($A \approx 90$) nuclei (§ 2.1.3) cannot be seen for all the cases (Figs. 8a-f). This is due to the low entropy ($\sim 10 N_A k$) of the shock-heated matter (without neutrino-heating), in which the α-rich freezeout (that can be seen in neutrino winds) is not of significance. The deficiency of r-process nuclei at $A \sim 115$ reflects the strong shell gap at $N = 50$ in the nuclear mass formula adopted to deduce the neutron-capture rates in this mass range. This valley might be fulfilled with another nuclear mass formula (see § 2.4) or another astrophysical site (e.g., neutrino winds, see Fig. 3c). Given the ejecta mass $M_{\rm ej}$ is reduced because of, e.g., a weaker explosion or fallback of the once ejected matter by the reverse shock, the prompt explosion from a collapsing O-Ne-Mg core considered here can be regarded as the origin of either "light" (cases a-b), "heavy" (case f) , or "all" (cases c-e) r-process nuclei. It is interesting to note that the production of thorium and uranium differs from model to model, even though the abundance pattern seems to be *universal* between the second and third r-process peaks. It should be noted that this event may not be the origin of nuclei lighter than $A \sim 70$. The mass of ejected iron is only $\approx 0.02 M_\odot$, and the production of α nuclei is negligible, since the outer envelope consists of, if survived from mass loss, only hydrogen and helium layers.

A serious problem in this scenario, other than *if it explodes*, is the *overproduction* of the "total" r-processed matter. While the abundance distribution is in good agreement with the solar r-process curve without an overproduction of $A \approx 90$ nuclei as seen in the neutrino wind, the ejected mass of r-processed matter in, e.g., case e in Fig. 8 is about $0.05 M_\odot$. This is more than two orders of magnitude larger than the requirement from Galactic chemical evolution (a few $10^{-4} M_\odot$). In addition, the remnant mass in this case results in only $1.13 M_\odot$ that is significantly smaller than the "typical" mass $1.4 M_\odot$, although a few NSs with measured masses are suspected to have such low masses (with relatively large errors, see 67). A possible explanation for this problem is that only a small fraction ($\sim 1\%$) of r-process material is ejected by "mixing-fallback" of the core matter (121; 122), wherein most of the r-process material falls back onto the proto-neutron star. An asymmetric explosion, such as that from rotating cores or jets may have a similar effect as the ejection of deep-interior material in a small amount. If this happened, the typical mass of the proto-NS ($\approx 1.4 M_\odot$) would be recovered.

2.3 Other Scenarios

The appearance of r-process elements in the old halo stars in the Galaxy no doubt demands the r-process nuclei to have a primary origin (§ 3), wherein the seed nuclei for neutron capture can be synthesized by itself as in the neutrino wind and the prompt explosion. In this regard, additional astrophysical sites that show some promise as the r-process origin currently suggested are the "NS mergers", the "accretion-induced collapses (AIC)", and the "collapsars".

Of particular importance among these scenarios would be the coalescence of two NSs (or of an NS and a black hole), i.e., the "NS merger", which might naturally provide the neutron-rich environment needed for r-process. The presence of double NS binaries with extremely short periods (e.g., 67) is an indirect, but unambiguous evidence that such events exist in reality, although its event rate is poorly known. So far, little effort has been devoted to the nucleosynthetic study in this event (74; 32; 40), which would be premature to make any firm predictions of its contribution to Galactic chemical evolution. Nevertheless, recent studies suggest a solar-like r-process abundance production for nuclei with $A > 130$ in such events (32; 40) and no lighter nuclei than $A \sim 70$ (40), which might be distinguishable from abundance determinations of extremely metal-poor halo stars.

An AIC of a (C-O or O-Ne-Mg) white dwarf in a close binary system (85) is an analogous event to a core-collapse SN, resulting in, perhaps, similar outcome to that of the neutrino wind or the prompt explosion. A lack of the outer envelope may result in, however, the production of no α and little iron-peak elements similar to the prompt explosion (96; 126). Note that the presence of a dense accretion disk around the core may help the matter to be neutron-rich even in the neutrino-heated ejecta. There has been, however, no r-process abundance prediction so far, and a quantitative study in the future is highly desired. A collapsar is also suspected to be an astrophysical r-process site, owing to its extremely high entropy along the polar direction as well as the dense accretion disk with low Y_e around the nascent black hole (70; 91). Since the central engine that drives the jets to induce a gamma-ray burst or a hypernova is still unknown, it would be too early to state any predictions here, and future quantitative studies are also desired.

2.4 Uncertainties in the nuclear data far from β-stability

Besides astrophysical conditions described above, another underlying difficulty for r-process calculations is due to the uncertainties in the theoretical predictions of nuclear data far from the β-stability, for which essentially no experi-

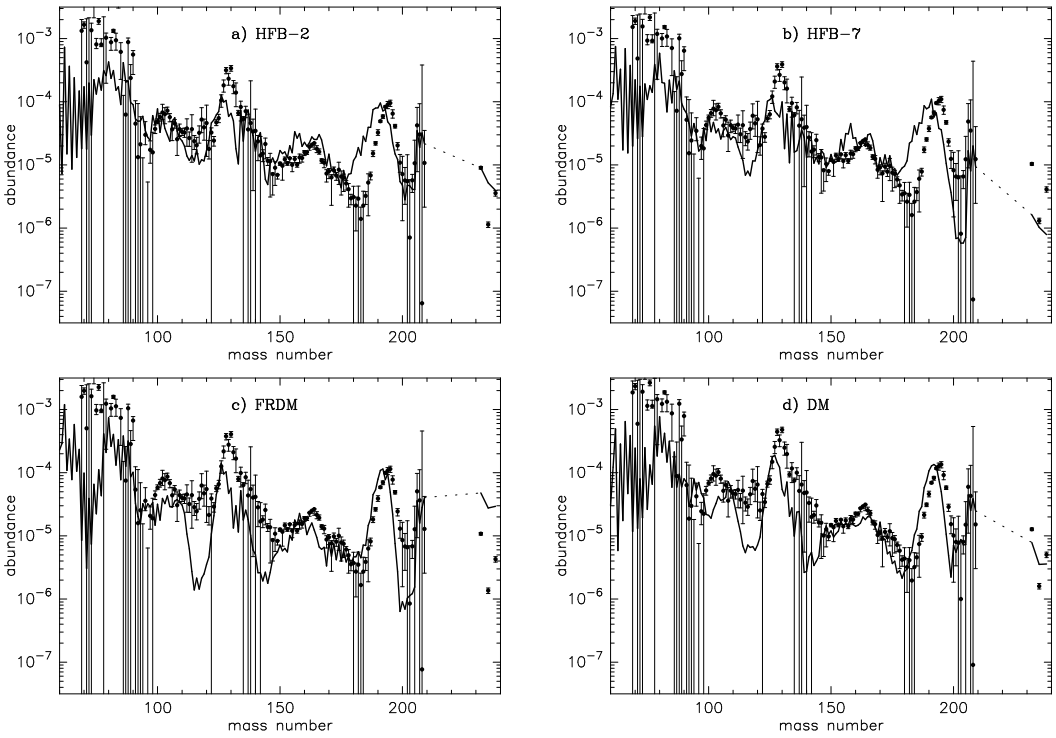

Fig. 9. Final mass-averaged r-process abundances (line) as a function of mass number obtained with various mass formulae; (a) HFB-2, (b) HFB-7, (c) FRDM, and (d) DM. These are compared with the solar r-process abundances (points), which are scaled to match the height of the third r-process peak.

mental data exist (for a recent review, see 69). In particular, mass predictions for neutron-rich nuclei play a key role since they affect all the nuclear quantities of relevance in the r-process, namely the neutron capture, photodisintegration and β-decay rates, as well as the fission probabilities.

Attempts to estimate nuclear masses go back to the liquid-drop Weizsäcker mass formula. Improvements to this original model have been brought little by little, leading to the development of macroscopic-microscopic mass formulae, such as the droplet model (e.g., 43, DM) and the "finite-range droplet model" (FRDM) of (83). In this framework, the macroscopic contribution to the masses and the microscopic corrections of phenomenological nature are treated independently, both parts being connected solely through a parameter fit to experimental masses. As a consequence, its reliability when extrapolating far from experimentally known masses is severely limited, despite the great empirical success of these formulae (e.g. FRDM fits the 2135 $Z \geq 8$ experimental masses (5) with an rms error of 0.676 MeV). A new major progress has been achieved recently within the Hartree-Fock-Bogoliubov (HFB) method (100; 38; 39; 41). It is now demonstrated that this fully microscopic approach, making use of a Skyrme force fitted to essentially all the experimentally known mass data, is not only feasible, but can successfully compete with the most accurate droplet-like formulae available nowadays (e.g., FRDM) in the repro-

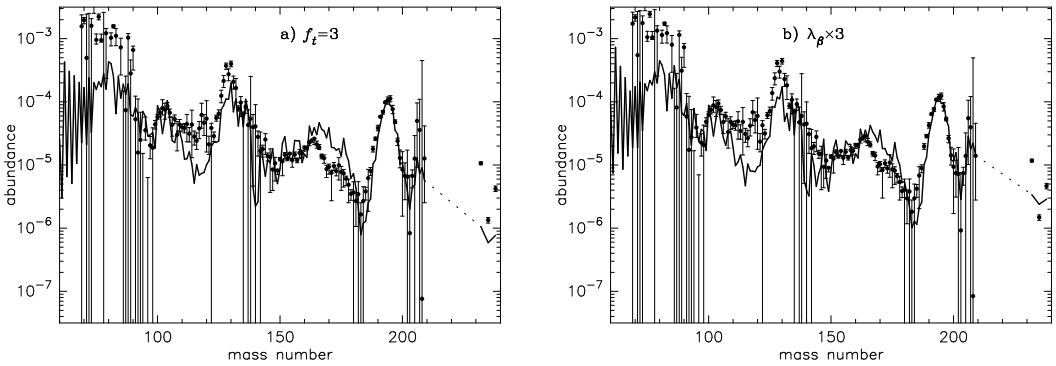

Fig. 10. Same as Fig. 9, but for (a) slow trajectories and (b) fast β-decay rates (a factor of three, see text) with the HFB-2 mass formula.

duction of measured masses (e.g., an rms error of the order of 0.674 MeV for the HFB-2 (38) mass table).

Most particularly, the HFB mass formulae show a weaker neutron-shell closure close to the neutron drip line with respect to droplet-like models such as FRDM. This effect can be seen in Fig. 9 that shows the results of r-process calculations with four sets of nuclear mass formulae HFB-2 (38), HFB-7 (40), FRDM (83), and DM (43), with the prompt explosion model described in § 2.2 (for more detail, see 127). Due to its weak shell effect at the neutron magic numbers in the neutron-rich region, the microscopic mass formulae (HFB-2 and HFB-7) give rise to a spread of the abundance distribution in the vicinity of the r-process peaks ($A = 130$ and 195). While this effect resolves the large underproduction at $A \approx 115$ and 140 obtained with droplet-type mass formulae (FRDM and DM), large deviations compared to the solar pattern are found near the third r-process peak. When using the droplet mass formulae, sharp r-process peaks are systematically found, owing to their strong shell effect for neutron magic numbers even in the neutron-rich region. However, due to the numerous uncertainties still affecting the astrophysics models as well as the prediction of extra nuclear ingredients, it would be highly premature to judge the quality of the mass formula on the basis of such a comparison.

For example, we find that abundance peaks similar to the one observed in the solar system could be recovered with the HFB-2 mass formula if the dynamical timescales of the mass trajectories are increased by a factor of three (without any change in the entropy, Fig. 10a) or by decreasing systematically the β-decay half-lives by the same factor (Fig. 10b). This is a consequence that the freezeout of (n, γ) and (γ, n) reactions takes place at higher temperature (and thus closer to the β-stability), where the shell gaps at neutron magic numbers are evident in the HFB-2 masses (for more detail, see 127). These changes might be conceivable when considering the current uncertainties in the astrophysics as well as in the nuclear β-decay model. Much effort in the astrophysics and nuclear modeling remain to be devoted to improve the

difficult description of the r-process nucleosynthesis.

3 Galactic Chemical Evolution

While no consensus has been achieved on the astrophysical r-process site from the nucleosynthetic point of view, Galactic chemical evolution studies provide several important clues to this puzzle from another point of view, when combined with recent comprehensive spectroscopic analyses of extremely metal-poor halo stars. Major issues here are threefold. First is the *universality* of the stellar abundance distributions that agree with the scaled solar r-process curve at least between the second and third r-process peaks ($Z \approx 56 - 78$). This implies uniqueness of the physical conditions to some extent, in which the r-process proceeds. Second is huge star-to-star *dispersion* of the r-process abundances relative to iron, which may pose a significant constraint on the stellar mass range of the SN progenitors as the origin of r-process nuclei. Third is the disagreement of the lighter ($Z < 56$) neutron-capture elements with the scaled solar r-process curve that match the heavier, which implies the presence of at least *two* r-process sites.

3.1 "Universality" of the r-Process Abundances

One of the most remarkable findings related to the spectroscopic studies of Galactic halo stars in the last decade is the discovery of several extremely metal-poor ([Fe/H][1] ~ -3), r-process-enhanced ([Eu/Fe][2] $\sim 1 - 2$) stars, whose abundances of neutron-capture elements are in excellent agreement with the scaled solar r-process curve (108; 20; 44; 26; 109; 48; 22). As can be seen in Fig. 11, the neutron-capture element abundances in CS 22892-052 ([Fe/H] $= -3.1$ and [Eu/Fe] $= 1.7$) (108; 109) show an outstanding concordance with the scaled solar r-process abundance curve, in particular between the second and third r-process peaks ($Z = 56-82$). The appearance of *purely* r-processed matter[3] in the atmosphere of such old halo stars in the Galaxy strongly support the idea that the production of r-process nuclei is associated to short-lived massive stars, perhaps, core-collapse SNe (119). Furthermore, the uniqueness of the abundance patterns of neutron-capture elements demonstrates the *uni-*

[1] $[A/B] \equiv \log(N_A/N_B) - \log(N_A/N_B)_\odot$, where N_A indicates abundance of A.
[2] Eu is often taken to be representative of r-process elements, since 94% of its solar abundance originates from r-process (4).
[3] s-process-enhanced, extremely metal-poor *carbon* stars are not considered here, whose atmosphere might have been polluted from the former AGB companions in binaries (129).

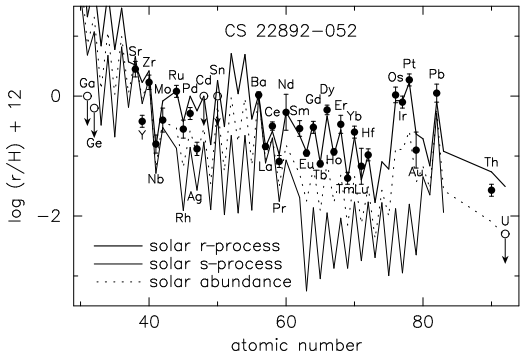

Fig. 11. Observed abundances in CS 22892-052 (109). The metallicity of this star is [Fe/H] = −3.1. Detected elements are shown as filled circles with error bars, and upper limits are denoted with open circles. The solar *r*-process (thick-solid line), *s*-process (thin-solid line), and the solar abundances (dotted line) (1) are vertically scaled to match the observed Ba abundance.

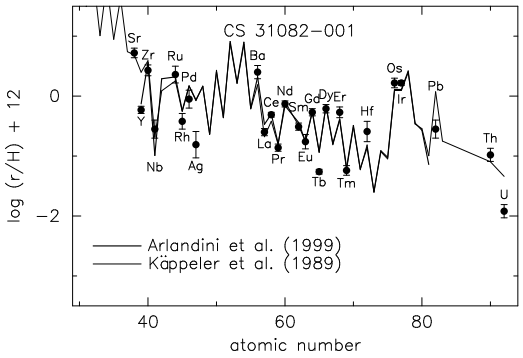

Fig. 12. Observed abundances in CS 31082-001 (44; 56; 90). The metallicity of this star is [Fe/H] = −2.9. Detected elements are shown as filled circles with error bars. The solar *r*-process abundances from Arlandini et al. (4, thick line) and Käppeler et al. (61, thin line) are vertically scaled to match the observed Eu abundance.

versality of the *r*-process nucleosynthesis that occurs in, perhaps, a unique astrophysical site.

Another notable discovery is the detection of uranium in CS 31082-001 ([Fe/H] = −2.9 and [Eu/Fe] = 1.6) (20; 44), which can be regarded as a precise cosmochronometer in addition to Th previously used for age dating (24; 25; 36) (§ 3.4). On the other hand, however, the significantly high Th and U (and low Pb) abundances compared to those in CS 22892-052 clearly show that the universality does *not* hold beyond the third *r*-process (Pt) peak, which makes the age dating assuming the "universality" of the *r*-process abundance pattern questionable. This *non-universality* of the *r*-process beyond the Pt-peak has been further confirmed by additional findings of Th-rich stars (48; 136).

It is not clear from currently available data that the *universality* holds down to the elements near the first *r*-process peak, e.g., Sr, Y, and Zr, owing to the deficiencies of a few elements between the first and second *r*-process peaks, as can be seen in Figs. 11 and 12. It should be noted that the *s*-process dominated elements in the solar system, e.g., Sr (85%), Y (92%), and Ba (81%), involve large uncertainties when deriving the *r*-process components from the observed solar values by subtracting the theoretically calculated *s*-process contribution (35). In fact, the deficiency of Y abundance is cured when adopting the recent data from Arlandini et al. (4) instead of the older table from Käppeler et al. (61), as can be seen in Fig. 12. The deficiency of Ag relative to the scaled solar *r*-process curve can be seen in *all* metal-poor stars that have its measured values (60; 54). Hence the low Ag abundance does not necessarily indicate the

break down of the universality below the second r-process peak as previously suggested (e.g., 109), although the reason of its deficiency is unknown [4].

3.2 "Dispersion" of the r-Process Abundances

Another striking feature of the observed neutron-capture element abundances in extremely metal-poor stars is their large dispersions that cannot be seen in any other elements (133; 72; 99). In Fig. 13, the observed Eu abundances (as representative of heavy r-process elements) relative to iron taken from the recent literature are plotted. The dispersion for the measured values ranges about two orders of magnitude at [Fe/H] ~ -3, which is in contrast to the exceedingly small scatters for α and iron-peak elements (21).

This large dispersion may be interpreted as a result of incomplete mixing of the interstellar medium (ISM) at the beginning of the Galaxy. In the *standard* chemical evolution models that are commonly used (e.g., 117), observed stellar compositions are taken to represent those of the ISM averaged over whole the Galaxy when the stars were formed. It may not be true, however, if star formations are affected by nearby SNe. The composition of the newly formed star must be a mixture of the low-metallicity ISM and the *single* (or a few) SN ejecta with the high metal content. In the following, our recent results of Galactic chemical evolution studies of r-process elements are presented, along with our recent spectroscopic analysis of several extremely metal-poor stars using SUBARU/HDS (see 51; 53; 54, for more detail). A few other recent studies that have taken the effect of inhomogeneity in ISM into account show qualitatively similar results (118; 120; 29; 3).

In our study, the evolutions of the ISM in the Galactic halo are calculated by a one-zone (i.e., *homogeneous*) model as in the *standard* approach, which loses gas through accretion onto the disk (51). The star formation and accretion rates are assumed to be proportional to the gas fraction of the halo. The star formations obey the Salpeter initial mass function in the mass range $0.05 - 60 M_{\odot}$. The coefficients for the accretion rate and the star formation rate are adjusted to fit to the observational data of [O/Fe] versus [Fe/H] (e.g., 7; 27) and the metallicity distribution of halo stars (101).

The chemical compositions of newly formed stars are determined as follows. We assume that star formation is initiated by SNe. An SN remnant is supposed to expand spherically until reaching the merge radius with the ISM (typically ~ 100 pc; 23). At this point, about $\sim 10^4 M_{\odot}$ of the ISM is swept up by the SN remnant. The composition of a formed star is then assumed to be the

[4] The uncertainty in deriving the solar r-process component of Ag abundance may be small (35), owing to its dominance (80%) in the solar system abundance.

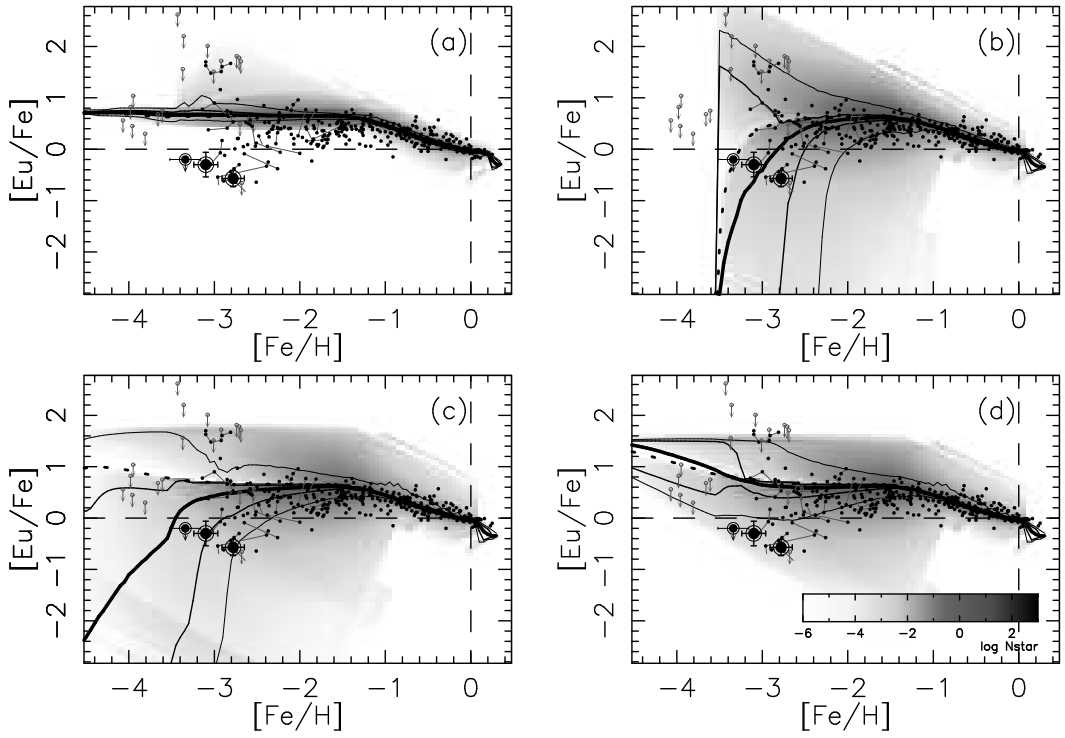

Fig. 13. Model predictions of [Eu/Fe] in stars as functions of [Fe/H] are compared with the recent observations. The r-process site is assumed to be SNe of (a) $\geq 10M_{\odot}$, (b) $8-10M_{\odot}$, (c) $20-25M_{\odot}$, and (d) $\geq 30M_{\odot}$. The predicted number density of stars per unit area is shown by the grey images. The average stellar abundance distributions are indicated by thick-solid lines with the 50% and 90% confidence intervals (solid and thin-solid lines, respectively). The average abundances of the ISM are denoted by the thick-dotted lines. The observed abundances taken from the recent literature (filled and open circles for measured values and upperlimits, respectively, 42; 72; 73; 133; 99; 107; 108; 131; 14; 34; 88; 59; 60; 30; 48) are plotted, along with our recent data (large double circles) obtained with SUBARU/HDS (53).

mass average of this "snowplowed" ISM and the *single* SN ejecta. The mass of the SN progenitor is chosen randomly but obeying the initial mass function. Contribution of this individual SN yield to the ISM is not considered here, whose evolution is calculated independently by the one-zone model.

The iron yields for Type II and Type Ia SNe are taken from (86) and (87), respectively. The possible metallicity effects are not considered here for simplicity [5]. The production of iron in $8-10M_{\odot}$ stars, which is estimated to be small by nucleosynthesis calculations (126), is neglected here. The r-process site is currently unknown, but *assumed* here to be the core-collapse SNe (either "neutrino winds" or "prompt explosions") from the stars of (a) $\geq 10M_{\odot}$

[5] A large metallicity dependence of the iron yield would result in too large scatters of α elements relative to iron (52), which conflicts with the recent spectroscopic studies of metal-poor stars (e.g., 21).

(all SNe), (b) $8-10M_\odot$ (low-mass end of SNe), (c) $20-25M_\odot$ (intermediate-mass SNe), and (d) ≥ 30 (high-mass end of SNe)[6]. Each case accounts for (a) 100%, (b) 28%, (c) 11%, and (d) 15 % of all SN events. The Eu yield is taken to be constant[7] for simplicity, over the stellar mass range for each, (a) $1.2\times10^{-7}M_\odot$, (b) $3.1\times10^{-7}M_\odot$, (c) $1.1\times10^{-6}M_\odot$, and (d) $7.8\times10^{-7}M_\odot$, which is scaled to reproduce the solar value [Eu/Fe] = [Fe/H] = 0, and to be zero outside of the range. It can be seen that the limited mass range demands the high r-process material ejected per event. The corresponding *total* mass of r-process nuclei for each case is about a few $10^{-5}M_\odot$ to a few $10^{-4}M_\odot$, which is in good agreement with theoretical estimates from nucleosynthesis calculations in neutrino winds (135; 124; 125).

For case a (Fig. 13a), the predicted area in which stars are detected (shown by the grey image) is small and close to the average stellar abundance (thick-solid line) and the ISM value (thick-dotted line). Most of the observed stars distribute out of its 90% confidence interval (thin-solid line). This is due to a weak dependence of the Eu/Fe value on the progenitor mass, since all SNe are assumed to be the r-process site. In fact, this is rather similar to the observed abundances of α elements with exceedingly small dispersion (e.g., Mg), which have only mild dependence of the yields on the progenitor mass. In contrast, large dispersions are predicted for cases b-d. This is explained as follows. The star formed by the SN that undergoes r-process inherits the large amount of Eu. This results in the higher [Eu/Fe] than the ISM value. On the other hand, the star formed by the SN without r-process but with Fe ejecta has the [Eu/Fe] value below the ISM line. As a result, a large dispersion of the [Eu/Fe] values appears. The dispersion converges as the metallicity increases, which also can be seen in the observed stars, since the formed stars in the high-metallicity ISM are less affected by the individual SNe.

Figs. 13a-d clearly demonstrate that the limited mass range ($\sim 10\%$ of all SN events) of the progenitor stars that undergo the r-process naturally explain the observed large star-to-star scatters of the r-process elements relative to iron. In addition, a small (or no) iron production strengthens the dispersion owing to the appearance of stars with high [Eu/Fe] values, which can be seen in case b. A significant difference among these three cases appears, however, in the areas with the sub-solar [Eu/Fe] (< 0) values near [Fe/H] $= -3$. Stars with low [Eu/Fe] values must appear if the r-process elements originate from

[6] These mass ranges are chosen as the representative four cases. A small shift of the range (e.g., $10-11M_\odot$ for case b or $25-30M_\odot$ for case c) would not change significantly the current results.

[7] In reality, the r-process yields must be dependent on the SN progenitor masses. A mild dependence over all the SN mass range would, however, result in only a small star-to-star scatter similar to Fig. 13a. A strong progenitor mass dependence of the Eu yield would have a similar effect to the restricted mass range with the constant Eu yield considered here (see, e.g., 120).

SNe near their lower-mass end (Fig. 13b) owing to their delayed appearances, as also predicted by an earlier work (71). On the other hand, few stars are expected to appear in this region for case d, since the ISM is initially enriched with the r-process elements by massive stars. Case c with the intermediate mass range of SNe lies between cases b and d. Most of the observed stars, in particular when including those with the lowest [Eu/Fe] values at [Fe/H] ~ -3 (large double circles in Fig. 13), locate near the average value (thick line) predicted in case b, distributing within the 50% confidence interval (Fig. 13b). For case c, most of these stars distribute below the average line, but still within the 90% confidence interval (Fig. 13c). For case d, many observed stars are out of the 90% confidence interval.

This might support the SNe near their lower-mass end, e.g., collapsing O-Ne-Mg cores from $8 - 10 M_{\odot}$ stars (§ 2.2), as the astrophysical r-process site, although its explosion mechanism (i.e., "prompt" or "delayed") cannot be constrained. The little production of α and iron-peak elements in this site (96; 126) is also consistent with the observed small scatters of these elements in extremely metal-poor stars (21), by adding only r-process elements to the formed star. It should be noted that the slightly shifted mass range, e.g., $10-11 M_{\odot}$, which corresponds to the SNe from collapsing *iron* cores near their low-mass end with the relatively small ejection of α and iron-peak elements, would result in a similar outcome. The SNe from more massive progenitors, e.g., $20-25 M_{\odot}$ (case c), as proposed to be a possible case in the neutrino wind scenario (§ 2.1.4), cannot be excluded either, with the current limited number of stars having the measured Eu values. Further detections of Eu in the stars at [Fe/H] < -3 without any selection biases, are highly desired. On the other hand, the SNe near their high mass end, which may include "pair-instability SNe" or "collapsars", are less likely to be the origin of heavy r-process nuclei. It is interesting to note that the large r-processed material per event owing to the limited mass range would increase the chance of direct detection of r-process elements in nearby SN remnants by future observations. In particular, detection of gamma-ray emission from the decay of r-process nuclei would prove that the SNe with certain masses are the r-process site (95; 126).

It should be cautioned that the ISM is assumed to be *homogeneous* in the current models, which must be *inhomogeneous* to some extent at the early Galactic history. The chemical evolution study with a fully inhomogeneous ISM model shows that the stars with low [Eu/Fe] values (such as in Fig. 13b) always appear as far as the SNe that undergo r-processing are restricted to a certain progenitor mass range, even if the range is assumed to the high-mass end ($20 - 50 M_{\odot}$, see Fig. 3 in 3). On the other hand, such a model results in large star-to-star scatters of other elements, e.g., [α/Fe] (2), which conflicts with the recent spectroscopic studies of extremely metal-poor stars (e.g., 21). This might imply that the ISM at the early Galaxy was efficiently mixed (i.e., close to the homogeneous ISM), as far as in the region where stars formed.

Future comprehensive studies of *inhomogeneous* Galactic chemical evolution that account for *both* the large scatters of [r/Fe] and the small scatters of [α/Fe] observed in extremely metal-poor stars (e.g., 52; 62; 63), as well as more measurements of neutron-capture elements in stars with [Fe/H] < -3, will be needed before drawing any firm conclusions.

If "NS mergers" instead of SNe were taken as the major r-process site in the current chemical evolution model, the result would be in disagreement with the observed stellar abundances, as examined in a recent work (3). The reason is that the expected small event rate $\sim 10^{-5}$ yr^{-1} (123) (i.e., the large r-process amount per event to be the dominant r-process origin) with the long period needed for a coalescence results in an extremely large scatter of [Eu/Fe] as well as a significant delay of its appearance. The same may hold for AICs, whose event rate is estimated to be similar (6). A word of caution is, however, required concerning the treatment of NS mergers here. The Galactic evolution of NS mergers (or AICs) as well as the nature of their remnants are highly uncertain. In addition, the NS mergers may not induce star formation as assumed for SNe owing to their smaller kinetic energy, and thus not necessarily lead to a large scatter of the r-process elements in stars. A lack of α and iron-peak elements in the ejecta of NS mergers (32; 40) (and of AICs, perhaps) with their uncertain Galactic evolution makes it quite difficult to determine *when* (or, at which metallicity) the observed stars received the r-process material from the remnants of NS mergers. Obviously, more studies are needed.

3.3 "Weak" r-Process

Besides highly r-process-enhanced stars as described in § 3.1, there are a significant number of stars (at [Fe/H] ~ -3) that show enhancements of *only* light r-process nuclei such as Sr, Y, and Zr (60; 54). In particular, a large dispersion has been found in [Sr/Ba] at low metallicity (99; 60; 48), suggesting that the lighter elements such as Sr have a different origin from the "main" r-process that produces Ba and heavier elements. This may be interpreted as a result of "weak" (or failed) r-processing with insufficient (or no) free neutrons at the beginning of r-process, in which only light r-process nuclei are produced as can be seen in Figs. 3a, 4, and 8a-b. HD 122563 (49) may be one of such stars that have abundance distribution of the weak r-process (Fig. 14). However, the boundary mass number that divides this "weak" r-process and the "main" r-process has been unknown, owing to a limited number of stars that have the measured abundances located between the first and second r-process peaks, e.g., Ru, Rh, Pd, and Ag. In the following, our recent results of Galactic chemical evolution are presented (54), which may enable us to determine the typical boundary of these two r-processes.

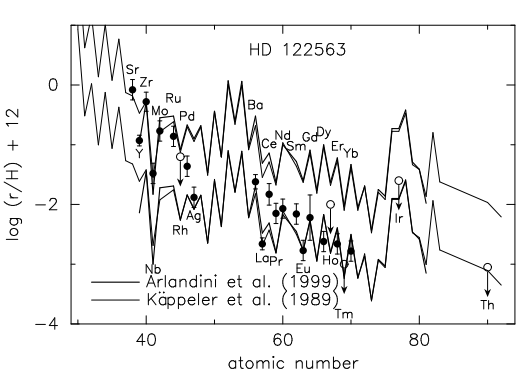

Fig. 14. Same as Fig. 12, but for HD 122563 (49). The metallicity of this star is [Fe/H] = −2.7. The solar *r*-process abundances are scaled to match the observed Zr and Eu abundances.

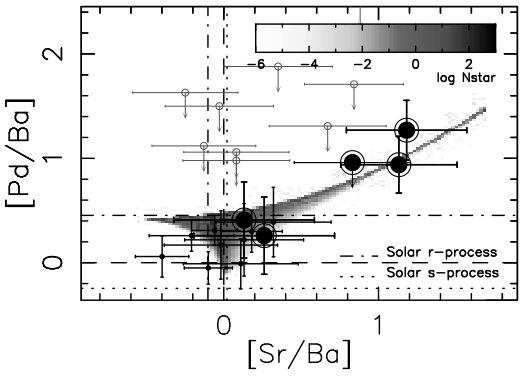

Fig. 15. Same as Fig. 13, but for [Pd/Ba] as a function of [Sr/Ba]. The large double circles indicate the stars obtained from our recent observations with SUBARU/HDS (54).

As representative of the weak and main *r*-processes and their intermediate, Sr, Ba[8], and Pd are taken here, respectively. Fig. 15 shows the [Pd/Ba] values as a function of [Sr/Ba] for extremely metal-poor stars ($-3.1 \leq$ [Fe/H] ≤ -2.3). Note that for stars in this metallicity range, no *s*-process contribution to Ba abundances are thought to occur, which is consistent with their mostly pure solar *r*-process ratios of Ba/Eu. The stellar sample is taken from the recent literature (44; 60; 109; 48), along with the five stars (large double circles) obtained from our recent observations with SUBARU/HDS (54). By definition, the [Sr/Ba] value increases with the contribution of weak *r*-process to the stellar abundances, when compared to the solar *r*-process value (dot-dashed line). The [Pd/Ba] value would increase linearly with [Sr/Ba] (with the slope of unity) if the Pd abundances were in proportion to those of Sr. On the other hand, [Pd/Ba] would show no increase if the Pd abundances were in proportion to those of Ba. The observed stars show a mild correlation with the slope less than unity, indicating Pd originates from *both* the weak and main *r*-processes.

The chemical evolution model described in § 3.2 (51) is used to determine the fractions of the weak r-process component to the *total* (i.e., both the weak and main *r*-processes) production of Sr, Pd, and Ba. Here, the weak and main *r*-process sites are assumed to be the stars of $8 - 10 M_{\odot}$ and $20 - 30 M_{\odot}$, respectively (changes of these mass ranges do not affect the result qualitatively, see 54). A reasonable fit to the observed stars can be obtained when the fractions of the weak *r*-process component to Sr, Pd, and Ba are assumed to be 60%, 10%, and 1%, respectively (Fig. 15). Thus, the *typical* weak *r*-process may synthesize mainly lighter nuclei up to $A \sim 100$ ($Z \sim 40$). However the number of the Sr-rich stars with the measured Pd abundances is so small (two measured values and one hard upper limit) that more observations will be

[8] There are few "weak" *r*-process stars with the measured values of Eu, but of Ba.

needed before drawing the conclusion. This boundary mass estimated here is significantly smaller than $A \sim 140$ that is suggested by the meteoritic analysis (130). It should be emphasized that the main r-process may produce *all* the r-process nuclei with the solar r-process-like distribution but, perhaps, with slightly underabundant lighter nuclei when subtracting the weak r-process component. As can be seen in Fig. 15, there is currently no observed star that shows strong excess of *only* heavy r-process elements with $A > 130$ (i.e., with significantly low [Sr/Ba] and [Pd/Ba] values compared to the solar r-process ratios) as suggested in previous studies (130; 32).

3.4 Cosmochronology

A few actinides such as ^{232}Th and ^{238}U are regarded as potentially useful cosmochronometers because their long radioactive decay half-lives (^{232}Th: 14.05 Gyr; ^{238}U: 4.468 Gyr) are significant fractions of the expected age of the universe. The excellent agreement of the relative abundances of neutron-capture elements in CS 22892-052 with the solar r-process pattern (§ 3.1) initially suggested that Th might serve as a precise cosmochronometer (108; 24; 58). The time that has passed since the production of Th observed now in the atmosphere of such an old halo star can be regarded as a hard lower limit on the age of the universe. One advantage of the actinide chronology is that, once the initial and current values of an actinide relative to an stable r-process element (r), e.g., Eu, in the star are specified, the age of the star depends only on the half-life of its actinide determined in the laboratory. That is, one is not forced to invoke complex models of Galactic chemical evolution, which no doubt involve large uncertainties in themselves.

The *initial* production ratio of Th/r has been usually determined by fitting theoretical nucleosynthesis results to the solar r-process pattern, with the assumption that the r-process pattern is *universal* over the actinide region in all astrophysical environments (e.g., 25; 36). However, there are an increasing number of evidences that the universality does not hold for actinides by the discoveries of Th-rich halo stars (44; 48; 136) whose Th/Eu values are higher than that of the solar r-process ratio. These *old* halo stars would be younger than the solar system if the initial Th/Eu were taken to be universal. Theoretical studies of r-process calculations also support the *non-universality* of the r-process abundances beyond the Pt-peak nuclei ($A \sim 200$), as can be seen in Fig. 8 (see also 125). Therefore, any age estimates that demand the universality of the r-process pattern may in fact be unreliable.

The discovery of the second highly r-process-enhanced halo star CS 31082-001 (20; 44) has provided a powerful new tool for age determination by virtue of the detection of uranium (37; 125; 103). Because the half-life of ^{238}U is

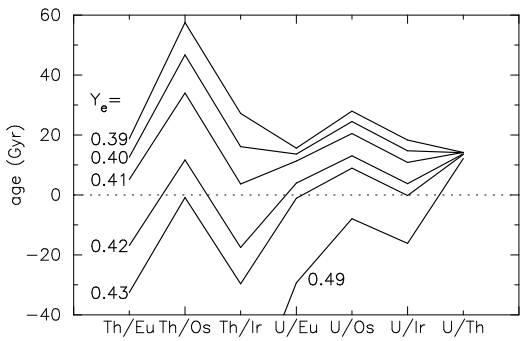

Fig. 16. Ages of CS 31082-001 derived from various chronometer pairs, comparing the abundances obtained from the spectroscopic analysis (44) and the theoretical estimate (125) based on the neutrino wind model as described in § 2.1. The robustness of the U-Th pair is clearly shown. The superiority of the U-r pairs compared to those of Th-r can also be seen.

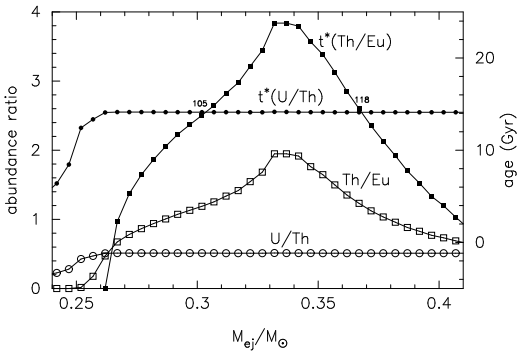

Fig. 17. Mass-integrated abundance ratios Th/Eu (open squares) and U/Th (open circles) from the surface of the core to the mass point $M_{\rm ej}$ in the prompt explosion model (126) as described in § 2.2. The surface of the O-Ne-Mg core is at mass coordinate zero. Ages of CS 31082-001, t^*(Th/Eu) (filled squares) and t^*(U/Th) (filled circles) inferred by these ratios, are also shown.

one-third that of ^{232}Th, uranium can, in principle, provide a far more precise cosmochronometer than thorium[9]. Furthermore, we are able to determine the initial r-process abundance curve in a star with the constraint that the ages derived from *both* the ratios Th/r and U/r (or U/Th) provide the same value. This "U-Th cosmochronology" that does not assume the universality of the r-process abundance pattern is a far more reliable age-dating technique than that with solely Th-r. Fig. 16 shows the ages of CS 31082-001 derived from various chronometer pairs, comparing the abundances obtained from the spectroscopic analysis (44) and the theoretical estimate (125) based on the neutrino wind model ($M = 2.0 M_\odot$ and $R_\nu = 10$ km) as described in § 2.1. Here, Y_e is taken to be a free parameter, which can be constrained to be ≈ 0.40 so as the ages obtained from, e.g., Th/Eu and U/Th give the same value. Fig. 17 shows the ages derived from the ratios Th/Eu and U/Th based on the prompt explosion model of a collapsing O-Ne-Mg core as described in § 2.2, as functions of the ejecta mass $M_{\rm ej}$. The free parameter here, $M_{\rm ej}$, can be constrained to be $0.30 M_\odot$ or $0.37 M_\odot$, where both ages from the ratios Th/Eu and U/Th give the same value. Interestingly, the ages of CS 31082-001 derived from the above two different astrophysical scenarios are the same – 14.1 ± 2.4 Gyr (the error only includes that arising from the observations). This demonstrates that chronometric estimates obtained using the U-Th pair are mostly independent of the astrophysical conditions considered, since these species separated by only two units in atomic number.

[9] ^{235}U may have mostly α decayed away because of its relatively short half-life (0.704 Gyr).

As far as the U-Th pair is concerned, therefore, the ingredients of nuclear data (37) as well as the estimated observational errors, rather than the r-process site, are crucial for the age determination. Note that the replacement of the nuclear mass formula (see § 2.4) from DM applied here (43) to FRDM (83) or the recent microscopic models (HFB-2 and HFB-7, 38; 100; 39) results in only small changes in age of the star ($14.0 - 14.3$ Gyr). The uncertainties in fission reactions may not affect the age significantly as far as the contribution of the fission fragment is not dominated in the final r-process abundances (37; 125; 126). It should be noted that there is a serious problem, that is, the measured Pb abundance is substantially lower than the scaled solar value as can be seen in Fig. 12 (90) and also than the theoretical estimates (126). Improved observational determination of the U/Th ratio in CS 31082-001 as well as the measurement of Bi (in addition to Pb) that is produced mainly by α-decay from actinides, and the identification of a greater number of highly r-process-enhanced, metal-poor stars, will be obviously needed before regarding the age-dating technique with the U-Th pair considered here to be confident.

4 Conclusions

The astrophysical r-process site is still unknown. Recent theoretical works of r-process calculations suggest some scenarios, in particular the "neutrino wind" or the "prompt explosion" arising from the core collapses of massive stars, or the "NS merger" to be promising, although all these involve severe problems that remain to be solved. On the other hand, recent Galactic chemical evolution studies as well as spectroscopic studies of extremely metal-poor halo stars imply the r-process origin to be the core-collapse SNe from the restricted progenitor-mass range (possibly near their lower-mass end). In addition, the presence of the "weak" r-process that produces only lighter r-process nuclei is suggested, while the "main" r-process may produce all r-process nuclei up to the actinides species. All these studies of r-process calculations and Galactic chemical evolution in the last decade have shown remarkable progresses toward better understanding of the r-process, and the ongoing works will shed light on this long-standing mystery.

Acknowledgements

This work was supported in part by a Grant-in-Aid for the Japan-France Integrated Action Program (SAKURA), awarded by the Japan Society for the Promotion of Science, and Scientific Research (17740108) from the Ministry of Education, Culture, Sports, Science, and Technology of Japan.

References

[1] Anders, E., & Grevesse, N. 1989, *Geochim. Cosmochim. Acta*, 53, 197

[2] Argast, D., Samland, M., Gerhard, O. E., Thielemann, F.-K. 2000, *Astron. Astrophys.*, 356, 873

[3] Argast, D., Samland, M., Thielemann, F.-K., & Qian, Y.-Z. 2004, *Astron. Astrophys.*, 416, 997

[4] Arlandini, C., Käppeler, F., Wisshak, K., Gallino, R., Lugaro, M., Busso, M., & Straniero, O., 1999, *Astrophys. J.*, 525, 886

[5] Audi, G., & Wapstra, A.H. 1995, *Nucl. Phys. A*, 595, 409

[6] Bailyn, C. D. & Grindlay, J. E. 1990, *Astrophys. J.*, 353, 159

[7] Barbuy, B. 1988, *Astron. Astrophys.*, 191, 121

[8] Baron, E. & Cooperstein, J. 1990, *Astrophys. J.*, 353, 597

[9] Bowers, R. & Wilson, J. R. 1982, *Astrophys. J.*, 263, 366

[10] Bruenn, S. W. 1989, *Astrophys. J.*, 340, 955

[11] Bruenn, S. W. 1989, *Astrophys. J.*, 341, 385

[12] Buras, R., Rampp, M., Janka, H. -Th, & Kifonidis, K. 2005, *Astron. Astrophys.*, submitted (astro-ph/0507135)

[13] Burbidge, E. M., Burbidge, G. R., Fowler, W. A., & Hoyle, F. 1957, *Rev. Mod. Phys.*, 29, 547

[14] Burris, D. L., Pilachowski, C. A., Armandroff, T. E., Sneden, C., Cowan, J. J., & Roe, H. 2000, *Astrophys. J.*, 544, 302

[15] Burrows, A. & Lattimer, J. M. 1983, *Astrophys. J.*, 270, 735

[16] Burrows, A. & Lattimer, J. M. 1985, *Astrophys. J.*, 299, L19

[17] Burrows, A., Hayes, J., & Fryxell, B. A. 1995, *Astrophys. J.*, 450, 830

[18] Cameron, A. G. W. 1957, *Chalk River Report*, CRL-41

[19] Cardall, C. Y. & Fuller, G. M. 1997, *Astrophys. J.*, 486, L111

[20] Cayrel, R., et al. 2001, *Nature*, 409, 691

[21] Cayrel, R., et al. 2004, *Astron. Astrophys.*, 416, 1117

[22] Christlieb, N., et al. 2004, *Astron. Astrophys.*, 428, 1027

[23] Cioffi, D. E., McKee, C. F., & Bertschinger, E. 1988, *Astrophys. J.*, 334, 252

[24] Cowan, J. J., McWilliam, A., Sneden, C., & Burris, D. L. 1997, *Astrophys. J.*, 480, 246

[25] Cowan, J. J., et al. 1999, *Astrophys. J.*, 521, 194

[26] Cowan, J. J., et al. 2002, *Astrophys. J.*, 572, 861

[27] Edvardsson, B., Andersen, J., Gustafsson, B., Lambert, D. L., Nissen, P. E., & Tomkin, J. 1993, *Astron. Astrophys.*, 275, 101

[28] Eldridge, J. J. & Tout, C. A. 2004, *Mon. Not. Roy. Astron. Soc.*, 353, 87

[29] Fields, B. D.,Truran, J. W.,& Cowan, J. J. 2002, *Astrophys. J.*, 575, 845

[30] François, P., et al. 2003, *Astron. Astrophys.*, 403, 1105

[31] Freiburghaus, C., et al. 1999, *Astrophys. J.*, 516, 381

[32] Freiburghaus, C., Rosswog, S., & Thielemann, F. -K. 1999, *Astrophys. J.*, 525, L121

[33] Fröhlich, et al. 2004, *Astrophys. J.*, in press

[34] Fulbright, J. P. 2000, *Astron. J.*, 120, 1841
[35] Goriely, S. 1997, *Astron. Astrophys.*, 325, 414
[36] Goriely, S. & Clerbaux, B. 1999, *Astron. Astrophys.*, 346, 798
[37] Goriely, S. & Arnould, M. 2001, *Astron. Astrophys.*, 379, 1113
[38] Goriely, S., Samyn, M., Heenen, P. -H., Pearson, J. M., & Tondeur, F. 2002, *Phys. Rev. C*, 66, 24326
[39] Goriely, S., Samyn, M., Bender, M., & Pearson, J. M. 2003, *Phys. Rev. C*, 68, 4325
[40] Goriely, S., Demetriou, P., Janka, H. -T., Pearson, J. M., Samyn, M. 2005, *Nucl. Phys. A*, 758, 587
[41] Goriely, S., Samyn, M., Pearson, J. M., & Onsi, M. 2005, *Nucl. Phys. A*, 750, 425
[42] Graton, R. G. & Sneden, C. 1994, *Astron. Astrophys.*, 287, 927
[43] Hilf, E. R., von Groote, H., & Takahashi, K. 1976, in Proc. Third International Conference on Nuclei Far from Stability (Geneva: CERN), 142
[44] Hill, V., et al. 2002, *Astron. Astrophys.*, 387, 560
[45] Hillebrandt, W., Takahashi, K., & Kodama, T. 1976, *Astron. Astrophys.*, 52, 63
[46] Hillebrandt, W., Nomoto, K., & Wolff, G. 1984, *Astron. Astrophys.*, 133, 175
[47] Hoffman, R. D., Woosley, S. E., Fuller, G. M., & Meyer, B. S. 1996, *Astrophys. J.*, 460, 478
[48] Honda, S., et al. 2004, *Astrophys. J.*, 607, 474
[49] Honda, S., Aoki, W., Ishimaru, Y., Wanajo, S., & Ryan, S. G., in preparation
[50] Iben, I. Jr., Ritossa, C., & García-Berro, E. 1997, *Astrophys. J.*, 489, 772
[51] Ishimaru, Y. & Wanajo, S. 1999, *Astrophys. J.*, 511, L33
[52] Ishimaru, Y., Prantzos, N., & Wanajo, S. 2003, *Nucl. Phys. A*, 718, 671
[53] Ishimaru, Y., Wanajo, S., Aoki, W., & Ryan, S. G. 2004, *Astrophys. J.*, 600, L47
[54] Ishimaru, Y., Wanajo, S., Aoki, & Ryan, S. G., & Prantzos, N. 2005, *Nucl. Phys. A*, 758, 603
[55] Ito, H., Yamada, S., Sumiyoshi, K., & Nagataki, S. 2005, *Prog. Theor. Phys.*, submitted (astro-ph/0508512)
[56] Ivarsson, S., et al. 2003, *Astron. Astrophys.*, 409, 1142
[57] Janka, H. -T., Buras, R., Kitaura Joyanes, F. S., Marek, A., Rampp, M., & Scheck, L. 2005, *Nucl. Phys. A*, 758, 19
[58] Johnson, J. A. & Bolte, M. 2001, *Astrophys. J.*, 554, 888
[59] Johnson, J. A. 2002, *Astrophys. J. Suppl.*, 139, 219
[60] Johnson, J. A. & Bolte, M. 2002, *Astrophys. J.*, 579, 616
[61] Käppeler, F., Beer, H., & Wisshak, K. 1989, Rep. Prog. Phys., 52, 945
[62] Karlsson, T. 2005, *Astron. Astrophys.*, 439, 93
[63] Karlsson, T. & Gustafsson, B. 2005, *Astron. Astrophys.*, 436, 879
[64] Kolbe, E., Langanke, K., & Fuller, G. M. 2004, *Phys. Rev. Lett.*, 92, 111101

[65] Langanke, K. & Martinez-Pinedo, G. 2000, *Nucl. Phys. A*, 673, 481
[66] Lattimer, J. M. & Prakash, M. 2001, *Astrophys. J.*, 550, 426
[67] Lattimer, J. M. & Prakash, M. 2004, *Science*, 304, 536
[68] Liebendörfer, M. 2004, private communication
[69] Lunney, D., Pearson, J. M., & Thibault, C. 2003, *Rev. Mod. Phys.*, 75, 1021
[70] MacFadyen, A. I. & Woosley, S. E. 1999, *Astrophys. J.*, 524, 262
[71] Mathews, G. J., Bazan, G., & Cowan, J. J. 1992, *Astrophys. J.*, 391, 719
[72] McWilliam, A., Preston, G. W., Sneden, C., & Searle, L. 1995, *Astron. J.*, 109, 2757
[73] McWilliam, A. 1998, *Astron. J.*, 115, 1640
[74] Meyer, B. S. 1989, *Astrophys. J.*, 343, 254
[75] Meyer, B. S., Mathews, G. J., Howard, W. M., Woosley, S. E., & Hoffman, R. D. 1992, *Astrophys. J.*, 399, 656
[76] Meyer, B. S. 1995, *Astrophys. J.*, 449, L55
[77] Meyer, B. S., McLaughlin, G. C., & Fuller, G. M. 1998, *Phys. Rev. C*, 58, 3696
[78] Fuller, G. M. & Meyer, B. S. 1995, *Astrophys. J.*, 453, 792
[79] McLaughlin, G. C. & Fuller, G. M. 1996, *Astrophys. J.*, 464, L143
[80] McLaughlin, G. C., Fuller, G. M., & Willson, J. R. 1996, *Astrophys. J.*, 472, 440
[81] McLaughlin, G. C. & Fuller, G. M. 1997, *Astrophys. J.*, 489, 766
[82] Miyaji, S. & Nomoto, K. 1987, *Astrophys. J.*, 318, 307
[83] Möller, P., Nix, J. R., Myers, W. D., & Swiatecki, W. J. 1995, At. Data Nucl. Data Tables, 59, 185
[84] Nomoto, K. 1984, *Astrophys. J.*, 277, 791
[85] Nomoto, K. & Kondo, Y. 1991, *Astrophys. J.*, 367, L19
[86] Nomoto, K., Hashimoto, M., Tsujimoto, T., Thielemann, F. -K., Kishimoto, N., Kubo, Y., & Nakasato, N. 1997, *Nucl. Phys. A*, 616, 79
[87] Nomoto, K., et al. 1997, *Nucl. Phys. A*, 621, 467
[88] Norris, J. E., Ryan, S. G., & Beers, T. C. 2001, *Astrophys. J.*, 561, 1034
[89] Otsuki, K., Tagoshi, H., Kajino, T., & Wanajo, S. 2000, *Astrophys. J.*, 533, 424
[90] Plez, B., et al. 2004, *Astron. Astrophys.*, 428, L9
[91] Pruet, J., Thompson, T. A., & Hoffman, R. D. 2004, *Astrophys. J.*, 606, 1006
[92] Pruet, J., Woosley, S. E., Buras, R., Janka, H. -T., & Hoffman, R. D. 2005, *Astrophys. J.*, 623, 325
[93] Qian, Y. -Z. & Woosley, S. E. 1996, *Astrophys. J.*, 471, 331
[94] Qian, Y. -Z., Haxton, W. C., Langanke, K., & Vogel, P. 1997, *Phys. Rev. C*, 55, 1532
[95] Qian, Y. -Z., Vogel, P., & Wasserburg, G. J. 2002, *Astrophys. J.*, 506, 868
[96] Qian, Y. -Z. & Wasserburg, G. J. 2003, *Astrophys. J.*, 588, 1099
[97] Ritossa, C., García-Berro, E., & Iben, I. Jr. 1996, *Astrophys. J.*, 460, 489
[98] Ritossa, C., García-Berro, E., & Iben, I. Jr. 1999, *Astrophys. J.*, 515, 381

[99] Ryan, S. G., Norris, J. E., & Beers, T. C. 1996, *Astrophys. J.*, 471, 254
[100] Samyn, M., Goriely, S., & Pearson, J. M., 2003, *Nucl. Phys. A*, 725, 69
[101] Sandage, A., & Fouts, G. 1987, *Astron. J.*, 97, 74
[102] Sato, K. 1974, Prog. Theor. Phys., 51, 726
[103] Schatz, H., Toenjes, R., Kratz, K.-L., Pfeiffer, B., Beers, T.C., Cowan, J.J., & Hill, V. 2002, *Astrophys. J.*, 579, 626
[104] Scheck, L., Plewa, T., Janka, H. -T., Kifonidis, K., & Müller, E. 2004, *Phys. Rev. Lett.*, 92, 0111031
[105] Schramm, D. N. 1973, *Astrophys. J.*, 185, 293
[106] Shen, H., Toki, H., Oyamatsu, K., & Sumiyoshi, K. 1998, *Nucl. Phys. A*, 637, 435
[107] Shetrone, M. D. 1996, *Astron. J.*, 112, 1517
[108] Sneden, C., McWilliam, A., Preston, G. W., Cowan, J. J., Burris, D. L., & Armosky, B. J. 1996, *Astrophys. J.*, 467, 819
[109] Sneden, C., et al. 2003, *Astrophys. J.*, 591, 936
[110] Sumiyoshi, K., Suzuki, H., Otsuki, K., Terasawa, M., & Yamada, S. 2000, *Pub. Astron. Soc. J.*, 52, 601
[111] Sumiyoshi, K., Terasawa, M., Mathews, G. J., Kajino, T., Yamada, S., & Suzuki, H. 2001, *Astrophys. J.*, 562, 880
[112] Suzuki, T. K. & Nagataki, S. 2005, *Astrophys. J.*, 628, 914
[113] Takahashi, K., Witti, J., & Janka, H. -Th. 1994, *Astron. Astrophys.*, 286, 857
[114] Terasawa, M., Langanke, K., Kajino, T., Mathews, G. J., & Kolbe, E. 2004, *Astrophys. J.*, 608, 470
[115] Thompson, T. A., Burrows, A., & Meyer, B. S. 2001, *Astrophys. J.*, 562, 887
[116] Thompson, T. A. 2003, *Astrophys. J.*, 585, L33
[117] Timmes, F. X., Woosley, S. E., & Weaver, T. A. 1995, *Astrophys. J. Suppl.*, 98, 617
[118] Travaglio, C., Galli, D., Gallino, R., Busso, M., Ferrini, F., Straniero, O. 1999, *Astrophys. J.*, 521, 691
[119] Truran, J. W. 1981, *Astron. Astrophys.*, 97, 391
[120] Tsujimoto, T., Shigeyama, T., & Yoshii, Y. 2000, *Astrophys. J.*, L531, 33
[121] Umeda, H. & Nomoto, K. 2002, *Astrophys. J.*, 565, 385
[122] Umeda, H. & Nomoto, K. 2003, *Nature*, 422, 871
[123] van den Heuvel, E. & Lorimer, D. 1996, *Mon. Not. Royal Astron. Soc.*, 283, L37
[124] Wanajo, S., Kajino, T., Mathews, G. J., & Otsuki, K. 2001, *Astrophys. J.*, 554, 578
[125] Wanajo, S., Itoh, N., Ishimaru, Y., Nozawa, S., & Beers, T. C. 2002, *Astrophys. J.*, 577, 853
[126] Wanajo, S., Tamamura, M., Itoh, N., Nomoto, K., Ishimaru, I., Beers, T. C., & Nozawa, S. 2003, *Astrophys. J.*, 593, 968
[127] Wanajo, S., Goriely, S., Samyn, M., & Itoh, N. 2004, *Astrophys. J.*, 606,

1057
[128] Wanajo, S. 2005, in preparation
[129] Wanajo, S., Nomoto, K., Iwamoto, N., Ishimaru, I., & Beers, T. C. 2006, *Astrophys. J.*, 637, in press (ApJ preprint doi:10.1086/'498293')
[130] Wasserburg, G. J., Busso, M., & Gallino, R. 1996, *Astrophys. J.*, 466, 109
[131] Westin, J.,Sneden, C., Gustafsson, B.,Cowan, J. J. , *Astrophys. J.*, 530, 783
[132] Wheeler, J. C., Cowan, J. J., & Hillebrandt, W. 1998, *Astrophys. J.*, 493, L101
[133] Woolf, V. M., Tomkin, J., & Lambert, D. L. 1995, *Astrophys. J.*, 453, 660
[134] Woosley, S. E. & Hoffman, R. D. 1992, *Astrophys. J.*, 395, 202
[135] Woosley, S. E., Wilson, J. R., Mathews, G. J., Hoffman, R. D., & Meyer, B. S. 1994, *Astrophys. J.*, 433, 229
[136] Yushchenko, A., et al. 2005, *Astron. Astrophys.*, 430, 255